Journal of *Marine Science and Engineering*

MDPI

Article

Physio-Chemical and Mineralogical Characteristics of Gas Hydrate-Bearing Sediments of the Kerala-Konkan, Krishna-Godavari, and Mahanadi Basins

Anupama Kumari [1,*], Chandrajit Balomajumder [1], Amit Arora [2], Gaurav Dixit [3] and Sina Rezaei Gomari [4,*]

[1] Indian Institute of Technology, Roorkee 247667, India; chandfch@iitr.ac.in
[2] Department of Chemical Engineering, Shaheed Bhagat Singh State University, Firozpur 152001, India; amitarora@sbsstc.ac.in or aroraamitlse@yahoo.com
[3] Gas Hydrate Research and Technology Centre, Panvel, Mumbai 410221, India; DIXIT_GAURAV@ongc.con.in
[4] Department of Chemical Engineering, School of Science Engineering and Design, Teesside University, Middlesbrough TS1 3BX, UK
* Correspondence: akumari@ch.iitr.ac.in (A.K.); s.rezaei-gomari@tees.ac.uk (S.R.G.)

Abstract: The characteristics of the hydrate-bearing sediments affect the formation and dissociation of gas hydrate in sediments. The mineral composition, their dispersion, and chemical composition of hydrate-bearing sediment samples plays a dominant role in the hydrate stability condition and its economic development. In this paper, the physical properties of hydrate-bearing sediment of India are compared with each other. The sediment samples are taken from the Krishan-Godavari basin (Depth—127.5 and 203.2 mbsf), Mahanadi basin (Depth—217.4 mbsf), and Kerala-Konkan basin (Depth—217.4 mbsf). The saturation of the gas hydrate observed at these sites is between 3 and 50%. Particle size is an important parameter of the sediments because it provides information on the transportation and deposition of sediment and the deposition history. In the present study, we investigated the mineralogy of hydrate-bearing sediments by chemical analysis and X-ray Diffraction. XRD, FTIR, and Raman Spectroscopy distinguished the mineralogical behavior of sediments. Quartz is the main mineral (66.8% approx.) observed in the gas hydrate-bearing sediments. The specific surface area was higher for the sediment sample from the Mahanadi basin, representing the sediments' dissipation degree. This characterization will give important information for the possible recovery of gas from Indian hydrate reservoirs by controlling the behavior of host sediment. SEM analysis shows the morphology of the sediments, which can affect the mechanical properties of the hydrate-bearing sediments. These properties can become the main parameters to consider for the design of suitable and economic dissociation techniques for gas hydrates formed in sediments.

Keywords: hydrates; sediment; mineralogy; hydrate basin; elemental analysis

check for updates

Citation: Kumari, A.; Balomajumder, C.; Arora, A.; Dixit, G.; Gomari, S.R. Physio-Chemical and Mineralogical Characteristics of Gas Hydrate-Bearing Sediments of the Kerala-Konkan, Krishna-Godavari, and Mahanadi Basins. *J. Mar. Sci. Eng.* **2021**, *9*, 808. https://doi.org/10.3390/jmse9080808

Academic Editor: Decheng Wan

Received: 1 July 2021
Accepted: 25 July 2021
Published: 27 July 2021

Publisher's Note: MDPI stays neutral with regard to jurisdictional claims in published maps and institutional affiliations.

Copyright: © 2021 by the authors. Licensee MDPI, Basel, Switzerland. This article is an open access article distributed under the terms and conditions of the Creative Commons Attribution (CC BY) license (https://creativecommons.org/licenses/by/4.0/).

1. Introduction

Gas hydrates are formed when the guest molecules of suitable size and shape are captured through van der Waals forces in the well-defined cages of host molecules [1]. The molecules of water and gas chemically interact to construct an ice-like crystalline structure [2], which is stable at an absolute pressure and temperature range [3]. The bottom of the stability area of hydrate structures is designated with the Bottom-Simulating Reflectors (BSR), which are parallel to the seafloor at a sub-bottom depth of a specific hundred meters [4,5]. These BSRs are formed by a sharp elastic contrast between the methane hydrates bearing and the underlying sediments, which are either brine or gas saturated [6]. Recently, hydrates have gathered so much recognition due to their environmental importance and new energy resources [7]. The enormous quantity of methane hydrates is located in the permafrost regions and the ocean bed [8,9]. The amount of energy in methane hydrate is significantly more considerable than the hydrocarbon deposits on earth [7]. There are several studies which have attempted to observe the properties of hydrate-bearing

sediments directly from cores. The various hydrate dissociation techniques are thermal stimulation, depressurization, chemical injection, and CO_2 sequestration [10,11].

Hydrates recovered from natural deposits display a wide range of growth habits and tend to be patchily distributed within the host sediment according to texture. The base of hydrate stability in the marine surface has often been found at the approximate conditions of pressure and temperature given by phase equilibria. The sediment somehow inhibits gas hydrate nucleation and growth in porous media. Natural gas hydrates formed in sediments are observed in permafrost onshore areas and in sediments of subsea areas, where natural gas hydrates are formed in the stability region of hydrates. Sediments with hydrates in offshore areas have been found in water deeper than 300 m generally, and their existence zone is from the seafloor downward some hundred meters depending on the local geothermal gradient [12]. Natural gas hydrates are the different forms of energy sources other than conventional sources such as oil and coal. It acts as a part of the sediment skeleton, which occurs in load bearing, pore filling, and cementing forms [13]. Hydrates are a metastable material which can also easily decompose as the temperature increases or pressure decreases. This classification has been done by observing the infrared and X-ray images of standard cores and the pressure cores, respectively, from the gas hydrate expeditions of marine gas hydrate. The grain-displacing veins of hydrate in mud has been recognized as the dominant factor to observe the significant difference between the concentration of hydrate calculated from cores, well log resistivity, and velocity by assuming an isotropic uniform distribution of hydrates in pore space [13]. The dissociation of solid-gas hydrates formed in sediments invokes complex chemical, physical, and mechanical interactions in hydrates, which pose significant challenges in the evolution of secure and economical technology for gas production. Hence, the production of gas from natural deposits of gas hydrates demands different knowledge and technologies. The essential parameters required in the numerical simulations for the gas hydrate dissociation are permeability, compressibility, index properties, and undrained shear strength. There are a number of papers on the characterization of natural hydrate sediments with and without gas hydrates and the effect of hydrate formation on the characteristics of sediments [14]. Winters et al. 2014 observed the characteristics of sediments from the Kerala-Konkan, Krishna-Godavari Andaman, and Mahanadi basins and showed the effect of the sediment's properties on the morphology, formation, and distribution of gas hydrate. They developed the connections between morphology and physical properties of hydrate reservoirs [15].

The physical properties of sediments give the basic understanding of the formation and dissociation methods of gas hydrates. The natural deposits of gas hydrates need the assessment of production rates, stability of wellbore, and flow assurance to establish a safe and efficient strategy for gas production. The basic criteria for the characterization of the physical behavior of sediments are to observe the physical properties, such as porosity, density, and grain size [1]. The marine sediments are classified based on the origin of the sediments, such as lithogeneous, biogeneous, and hydrogenous. The sources of these types of sediments are volcanic and terrestrial, the marine organism remains, and seawater precipitates. Most of the marine sediments are observed along the continental areas originated from terrestrial sources. The production potential of the natural deposits of gas hydrates formed in marine sediments is the latest interesting research topic. There are studies that focus on finding the relation between the physical properties of the host sediments and the nature of the formation of hydrates. The inherent physical properties of the host sediment affect the morphology, location, and nature of the in situ hydrate. Winter et al. 2014 showed that the production potential of naturally formed gas hydrates could be influenced by porosity, permeability, and sedimentation rate other than the grain size [15]. Seo et al. 2009 predicted that the rheology and mineralogy of the clayey sediment affect the efficiency of methane production from marine sediments. The mineralogy and rheology of sediments have an important role during the formation and dissociation of in situ gas hydrate [15].

When the molecules of gas hydrates are trapped in the pore space of the marine sediments, the bulk physical properties of the sediments can be greatly affected. The electrical resistivity is the most influenced properties of the sediments from several other in situ physical properties. Hydrate-occupying sediments show comparatively large resistivity relative to the sediments without hydrate. Hence, the quantity of gas hydrates in the sedimentary part can be evaluated by a downhole resistivity log. An increase in electrical resistivity value was observed in the hydrate-bearing sediments from the Krishna-Godavari (KG) basin during the National Gas Hydrate Program (NGHP-01). This observation is useful to analyze the efficiency of in situ electrothermal heating during the dissociation process of hydrates [16]. The gas hydrate formation in the marine sediments can influence some of the physical properties of sediment and the difference in the properties can be discovered by field measurements and downhole logs [17].

Dong et al. 2020 indicated that hydrate with high saturation indicates a strain-softening brittle mode, and low saturation indicates a strain-hardening ductile failure mode [18]. Nair et al. 2016 studied the kinetics of methane gas hydrate formed in the porous media to understand the formation and dissociation behavior. They also examined the effect of the size of silica sand on the hydrate formation and concluded that the gas consumption in the smaller-sized sand particles is higher than the larger-sized sand particles. They also concluded that the recovery of gas and rate of dissociation is higher in the smaller-sized sand particles than the bigger-sized sand particles. Stoll and Bryan 1979 conducted experiments to determine the thermal conductivity and acoustic wave velocity in hydrates and sediments after the formation of hydrates. They observed a decrease in the thermal conductivity of sediments after the formation of hydrates [19,20]. Mahabadi et al. 2019 showed that the permeability of hydrate occupied sediments affects the dissociation of hydrate as well as the rate and efficiency of production [21]. Wang et al. 2020 studied the mechanical and physical properties of the overburden layer of sediments from the South China Sea, such as particle and pore size distribution, water content, specific surface area, compositions of minerals and chemicals [22]. The particle size of the clayey sediments will affect the induction and growth rate of hydrate. The interlayer structure and surface chemistry of the host sediments have a significant impact on the formation and dissociation of gas hydrates. The transport of these interlayer species through the clay is attributed to a complex interaction of the host molecule with sediments depending on the solid surface characteristics, such as surface charge, surface area, etc., in the suspensions of sediment. In clay type of materials stacking layers forms interlayers into which water molecules gets adsorbed resulting into hydrogen bonds formation. The surfaces of clay minerals having stacked silicate sheets have a net negative charge. It has been revealed in the literature that the few reactive sites present on the clay mineral surfaces are responsible for the promotional effect of formation by facilitating nucleation sites and well-ordered hydrate [23,24].

The flow behavior of sediments containing clay and silt will change shear thickening from shear thinning after an increase in the particle size. An increase in the saturation of hydrate can increase the strength of sediments. The stability of gas hydrates can be affected by the salinity of pore water [25]. Increase in the salinity of pore water can decrease the hydrate formation temperature. The hydrate formation and inhibition can be affected by the reduced water quantity in the clays. Uchida et al. 2004 observed that increased water content would increase hydrate accumulation [26]. Winters et al. 2004 concluded that the gas hydrates formed in natural sediments and in the laboratory have different physical properties [27]. Sun et al. 2019 performed a numerical simulation by a two-layer model and showed that the multi-physical responses are related to different material properties of the two layers [28]. Hyodo et al. 2014 investigated the mechanical behavior of CO_2 and CH_4 hydrate-bearing sediments [29]. The origin diversity of the clay and its physical and chemical characteristics can promote or inhibit or have no influence on hydrate stability. The hydrate formation process in sediments can also be affected by the type of mineral present in the sediments because the minerals present in the sediment can

affect the rheological properties of sediments. The hydrate-bearing sediments can show a significantly high strength. The shear strength of sediment can increase and effective stress can decrease because of the hydrate formation in sediments. The decrease in the effective stress can result in instability in the seafloor and leads to the various geohazards and can also influence the methane production [16]. Zhang et al. 2011 studied the effect of hydrate saturation and conversion ratio of water to hydrate, as well as the effect of grain size of the sand on the hydrate formation. They concluded that the conversion ratio has a significant role in distributing hydrate in sediment pores [30].

The National Gas Hydrate Program Expedition (NGHP) was organized to observe the existence of gas hydrate next to the Andaman convergent margin and the passive continental margin of the Indian Peninsula. This program's special attention was to interpret the geochemical and geologic dominance on the availability of gas hydrate. This program proved the existence of hydrates in the Krishna-Godavari, Kerala-Konkan, Andaman and Mahanadi basins. One of the thickest gas hydrate accumulations has been uncovered in the Krishna-Godavari basin and one of the deepest and thickest stability zones of gas hydrates in the world was discovered in the Andaman Sea. A total of 21 sites has been located, i.e., 15 sites in Krishna-Godavari, 1 site in Kerala-Konkan, 1 site in Andaman deep offshore, and 4 sites in Mahanadi. During this program, it was observed that the concentrated gas hydrate was related with the fractures mostly and for some restricted specimen by coarser grained sediments, i.e., mostly sand-rich type sediments [31]. The Krishna-Godavari basin has Class 4 type natural deposits, which have low methane hydrate saturation (<10%) layer and no impermeable layers [32].

This paper presents and compares the analysis of 10 physical properties of gas hydrate-bearing sediments recovered from natural gas hydrate reservoirs of India during National Gas Hydrate Program (NGHP). All sediment samples used for the study in this paper did not contain gas hydrate at the time of analysis. The properties of gas hydrate-bearing sediments without hydrate are still important since they can disturb the formation conditions of gas hydrates in clayey sediments. We have analyzed the properties of gas hydrate-bearing sediments, such as conductivity, pH, salinity, Total Dissolved Solids, Water Content, Density, Porosity, and Total Organic Carbon, of natural gas hydrate reservoirs recovered in India. The mineralogical and physio-chemical characteristics of gas hydrate-bearing sediment samples can help to develop economic dissociation technology for gas hydrates.

1.1. Bottom-Simulating Reflector (BSR)

Methane hydrate is stable inside the temperature range that prevails on the ocean floors at water pressures. After the formation of methane hydrate in sediments, the sediments' temperature increases with depth, leading to the instability of hydrates below the ocean floor at a few hundred meters [4]. The lower boundary formed at this depth is called the Bottom-Simulating Seismic Reflector (BSR). The identification of BSR gives the quantity of hydrate and recoverability (strength and permeability) and mobility of hydrate [4].

In the BSR detection method, a sonic wave penetrates and is reflected back from the ocean floor within some time. The velocity contrast below the ocean floor changes the density of the material. BSR with hydrates gives the designations of velocity contrast between the velocity in hydrate containing gas and sediments. This gives a sharp diminish and increase in sonic compression velocity and shear velocity, respectively. Hyndaman and Spence (1992) concluded that about 1/3rd of the pore space should be occupied with hydrate for the BSR identification [33,34]. The thickness of the stability zone of hydrates in marine sediments depends on the water depth, temperature of the seafloor, and geothermal gradient [34,35]. Umashankar concluded that the nature of BSR could be affected by sedimentation patterns parallel to the seafloor because gas hydrate in sediments can increase the electrical resistivity. Permeability reduces after the agglomeration of hydrate in sediments [36]. Permeability can also be related to velocity depending on the situation of gas hydrate formation [37].

1.2. Geographical Overview

A geographical overview of natural gas hydrate reservoirs in India is shown in Figure 1, which consists of locating the sites in Krishna-Godavari, Kerala-Konkan, Andaman deep offshore, and Mahanadi.

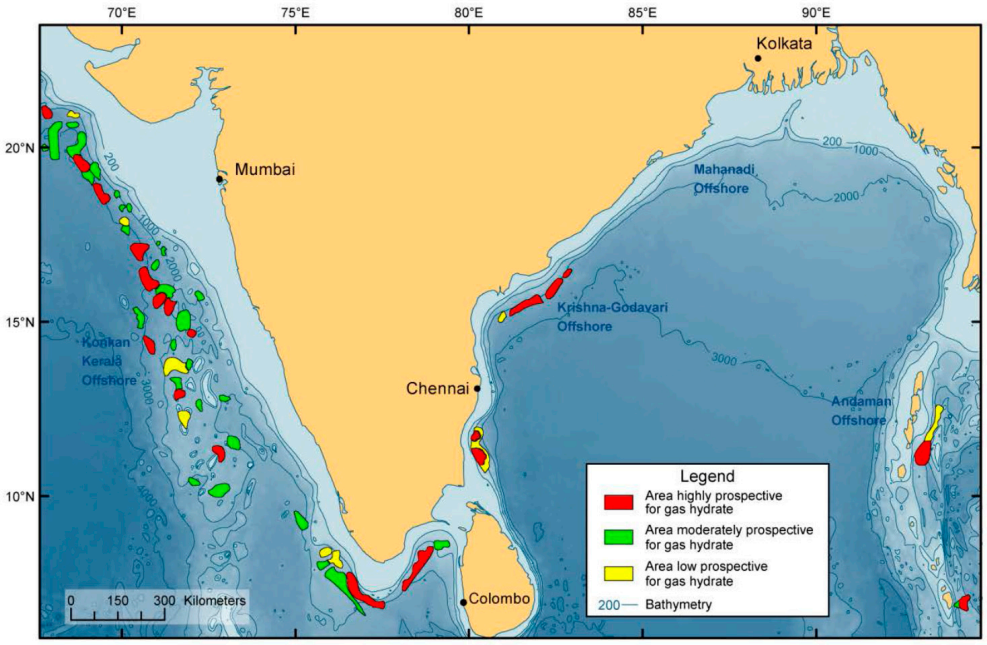

Figure 1. Locations of natural gas hydrate reservoirs observed in India [31].

1.2.1. Krishna-Godavari Basin

The Krishna and Godavari rivers form an extensive deltaic plain in Andhrapradesh and nearby areas of the Bay of Bengal. These rivers eject their water in this delta and form the Krishna-Godavari basin. This basin is located on the east coast of India and covers an area of 15,000 km^2 onshore and 25,000 km^2 offshore. This basin has 5 km thick sediments with extensive Carboniferous deposition to Pleistocene deposition. The basin was established by the splitting of the eastern continental side of the Indian Craton in the initial Mesozoic. The maximum thickness of the sediments in the basin is 5000 m, and the controlling factor for this thickness is the presence of a long linear Gondwana Rift valley. The entrapments of hydrocarbons are anticipated from Permo-Triassic to Pliocene sediments [38].

1.2.2. Mahanadi Basin

The Mahanadi basin originates from the rifting and breakup of Gondwana Land, situated on the east coast of India, covering an area of 14,000 km^2 in the shallow offshore area. The on-land part is restricted to the northwest and west through Pre-Cambrian outcrops, which belong to the Indian Crystalline aegis. The Onshore Mahanadi basin is situated in the Orissa, but the shallow offshore portion lies off in the Andhra Pradesh coast and Orissa. The basin lies between 80°30 to 86°50 east longitude and 19°21 to 23°35 north latitude. It covers the area in Madhya Pradesh, Orissa, Bihar, and Maharashtra states. The generalized Litho-Stratigraphic column of the Mahanadi shallow offshore basin consists of sands, clays, and silts. The temperature gradient in the onshore and offshore basin is found to be >2.5/100 m. The presence of organic matter and stratigraphic and structural traps in the basin indicate the hydrocarbon potential of the basin. The presence of coarse-grained sandstones confirmed the potential of sediments to host the hydrocarbons. The Mahanadi basin has the potential for the formation of gas hydrates due to the enormous volume of coarse-grained sediment and organic-rich sediments from the Brahmani and Mahanadi Rivers [39].

1.2.3. Kerala-Konkan Basin

The Kerala-Konkan basin is situated at 16° N latitude in the south. This offshore KK basin built the southern segment of the western continental edge of India and is distributed from Goato Cape Comorin. This basin is extending to the Arabian Abyssal Plain on the western side and is surrounded by a peninsular shield. These sediments contains sandstones, siltstones, shales and clay stones, argillaceous limestones, carbonate, white and grey clays, lignites, white plastic clays, peat/lignite, grey pebbly, coarse sands and mottled clays [38]. The basin is distributed in an area of 5.8×10^5 km^2 and the main sources of sediments in the Arabian Sea are the Indus River, which discharges in the northernmost part of the Arabian Sea and the Tapti and Narmada Rivers and ends in the Gulf of Combay. The Kerala-Konkan basin contains 109,000 km^3 Cenozoic sediments [40]. The sediments on the west coast are primarily globigerina clay [39]. The Kerala-Konkan basin has gained much interest because of its probable hydrocarbon potential [41].

1.2.4. Andaman Basin

The Andaman basin covers an area of 8×10^5 km^2 and is detached from the Bay of Bengal through the Andaman Nicobar Ridge. This basin extends 1200 km southward to Sumatra and the Malacca strait from the Irrawaddy delta coast of Burma. The principle source of sediments of the Andaman basin is the Irrawaddy River that contains silt and clay. The Irrawaddy River flows by way of central Myanmar and finishes in the northern Andaman Sea. Sediment core from the Andaman Sea contains terrigenous nannofossil carbonate and muddy clay [42].

2. Material and Methods

2.1. Preparation of Sample

The sediment samples were taken from the Mahanadi (Depth—217.4 mbsf, Hydrate Saturation—>50%, Sea Floor Temperature—2.4 °C), Kerala-Konkan (Depth—246.8 mbsf, Hydrate Saturation—15%), and Krishna-Godavari (Depth—127.5 and 203.2 mbsf, Hydrate Saturation—3 to 39%) basins in the Bay of Bengal by the Gas Hydrate Research and Technology Center (GHRTC), Panvel, Mumbai, INDIA. The samples were dried to remove moisture, and the physical appearance of sediment in raw and powder form is shown in Figure 2. The sediment samples have been transformed into powder form by a mortar. The different concentration of sediment samples was prepared to measure physical properties such as pH and TDS by dissolving it in a known quantity of Millipore water.

2.2. Experimental Setup

Particle Size Analysis (PSD), Scanning Electron Microscopy (SEM), X-ray Diffraction (XRD), Fourier Transform Infrared Spectroscopy, inductively coupled plasma mass spectrometry (ICPMS), Cation Exchange Capacities and Specific Areas, Total Dissolved Solids (TDS), Salinity, pH, Total Organic Carbon (TOC), Conductivity, and Raman Spectroscopy were performed to investigate the physical and mineralogical characteristics of gas hydrate-bearing sediments. The name of the equipment used for different tests is given in Table 1.

Site Location—Krishna-Godavari (KG(1a)) NGHP-02-19
Depth—127.5 mbsf

Site Location—Krishna-Godavari (KG(1b)) NGHP-02-19
Depth—203.2 mbsf

Site Location—Mahanadi NGHP-01-19
Depth—217.4 mbsf

Figure 2. *Cont.*

Site Location—Kerala-Konkan (KK) NGHP-01-01
Depth—246.8 mbsf

Figure 2. Hydrate-bearing sediment samples.

Table 1. Testing equipment used for different characteristics of hydrate-bearing sediments.

S.No.	Equipment Name	Company/Model No.	Characteristics of Hydrate-Bearing Sediments
1	Multi-Parameter Measuring Device	Model No.-KI-266A, Khera Instruments, Delhi, India	Physical Properties (pH, TDS, Salinity)
2	TOC Analyzer	Shimadzu, TOC-L, Kyoto, Japan	Total Organic Carbon
3	Oven Drying and Gas Pycnometer	Ultrapyc 5000, Anton Paar, Graz, Austria	Water Content, Density, Porosity
4	Inductively Coupled Plasma Spectrometer (ICPMS)	Perkin Elmer, ELAN DRC-e-2004, Boston, MA, USA	Elemental Analysis
5	Laser Particle Size Analyzer	HORIBA Scientific, nanopartica, Nano, Particle Analyzer, SZ-100, Osaka, Japan	Particle Size Distribution
6	BET	Micromeritics Asap 2060, Norcross, GA, USA	Specific Surface Area
7	Scanning Electron Microscope (SEM)	TESCAN MIRA3 FEG-SEM, Brno, Czech Republic	Shape and Surface Texture
8	X-ray Diffraction	Bruker, D8-Advance, 2008	Mineral Identification
9	Fourier Transform Infrared Spectroscopy	JASCO, FT/IR-6700 FT-IR Spectrometer, Tokyo, Japan	Mineral Identification
10	Raman Spectroscopy	Renishaw invia Raman Microscope instrument (Edinburgh, UK)	Structural Identification

3. Results and Discussion

3.1. Physical Properties of Sediment Samples

The physical properties of the sediment sample were performed as given in [43] and listed in Table 2. As shown in Table 2, the Total Organic Carbon content is higher for hydrate-bearing sediments from the Kerala-Konkan basin. The conductivity, pH, and salinity of hydrate-bearing sediments are higher for the Andaman basin [44]. The water content, density, and porosity are higher for the sediments from the Krishna-Godavari basin at 127.5 mbsf and lower for sediments from the Kerala-Konkan basin. The strength of the sediment samples increases as the water content of the sediment samples decreases. From the data, it can been observed that the sediment sample from the KK basin has the least percentage of water content and sediment sample, while KG(1a) contains the higher percentage of water content as compared to other sediment samples. Hence, the strength of the sediment sample from the KK basin is higher and the strength of the sediment sample

from the KG(1a) basin is lower. The decreasing order of strength of sediment samples is KK > Mahanadi > KG(1b) > KG(1a).

Table 2. Physical properties of sediment samples.

Sampling Locations	Water Content (%)	Density (g/cm^3)	Porosity (%)	Conductivity (mS/cm)	Salinity (ppt)	TDS (ppt)	TOC (ppm)	pH
KG(1a)	87.4	1.74	69.84	15.74	11.61	10.17	506.8	6.76
KG(1a)	78.8	1.67	67.62	14.93	11.28	9.78	146.24	6.71
Mahanadi	76.32	1.73	66.91	10.90	8.28	7.11	414.4	6.10
KK	67.2	1.61	64.03	8.78	6.52	5.63	3760.8	6.97

3.2. Particle Size Analyzer (PSA)

The particle size analysis of the hydrate-bearing sediment samples is shown in Figure 3 and Table 3. According to the results of NGHP, the sediment of Indian gas hydrate reservoirs is mainly of clay and silt type. The sand, silt, and clay particles are differentiated based on their particle size. The particle size of sand is large (0.1–2 nm), while the particle size of the clay is extremely fine (<0.002 mm) and the particle size of the silt is in between that of clay and sand (0.002–0.05 mm) [45].

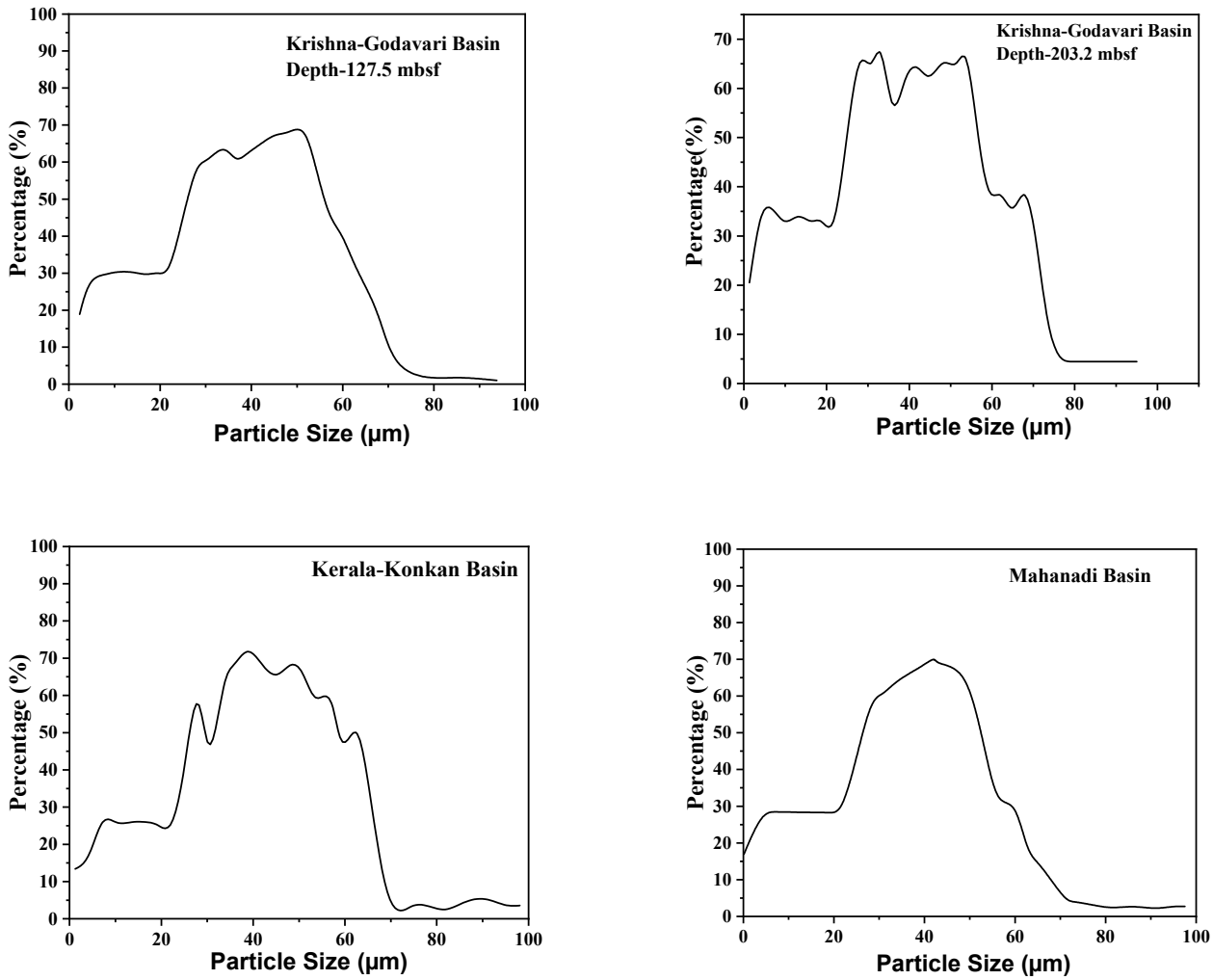

Figure 3. Particle size analysis of hydrate-bearing sediments.

Table 3. Minimum and maximum value of particle size diameter.

Sediments		D_{10}	D_{50}	D_{90} (μm)	Sediments		D_{10}	D_{50}	D_{90} (μm)
KG(1a)	min.	0.52	1.63	3.52	KK	min.	0.48	1.79	3.81
	max.	2.75	58.8	678.3		max.	2.99	13.2	278.01
KG(1b)	min.	0.63	1.69	4.54	Mahanadi	min.	0.51	1.72	3.46
	max.	2.89	144.9	682.8		max.	2.50	58.7	282.1

When the sediments contain clay particles, the dispersion of sediments will occur. When the sediments are mixed with water, the clay particles are loosened and the soil separates into single particles [46]. The asymmetrical polymodal distribution of sediment samples with the inflection points is shown in Figure 3. The sediment from the Krishna-Godavari basin at a depth of 127.5 mbsf shows the inflection points at around 38 and 36 μm, but the sediment from the Krishna-Godavari basin at a depth of 203.2 mbsf shows the inflection points at around 9.5, 30, 45, and 64 μm. The sediment from the Kerala-Konkan basin shows the inflection points at around 9.7, 25, 37, 43, 56, and 61 μm. The sediment from the Mahanadi basin shows the inflection points at around 8.7, 42, and 60 μm. The distribution width of the sample can be determined by the values of D_{10}, D_{50}, and D_{90}. These values give the diameter at which 10, 50, and 90% of the population is lower than the given value (Table 3). The sediments from the Krishna-Godavari basin are of clay with limited sand/silt bed type, but the sediments from the Mahanadi basin are not of silt/sand bed type. The gas hydrate-bearing sediments from the Kerala-Konkan basin are of a carbonate-rich type. Sediments of the Andaman basin mainly have clay/silt, volcanic ash bed type [44]. From Figure 3, it is confirmed that the sediment sample is of silt, sand, and clay type. The particle size of the sediment plays an essential role during the formation and dissociation of gas hydrates formed in sediment. This will affect the induction and growth rate of hydrates in sediments. The rate of hydrate induction in the small-sized particles of sediment is higher than particles of a large size. The unequal distribution of particle size in natural sediments also affects the equilibrium conditions of naturally formed deposits of methane hydrate. From the size of the sediments, it has been confirmed that the sediments sample are of fine/very fine sand, coarse, medium, fine, and very fine silt and clay types. The hydrate stability temperature in porous materials is high as compared to the bulk water. The particle size effect of sediment can be related by the proportion effect of bulk water [47]. The restricted water in porous sediments has different physical and chemical properties than bulk water [47]. The percentage of silt, clay, and sand particles was observed by the Hydrometer method (Table 4) [48]. The particle size of the hydrate-bearing sediment samples affects the time of nucleation and saturation of hydrate. The formation of hydrate may be easier in sediments of smaller particle sizes [49]. The dispersion of small-sized sediment is affected by the induced flocculation, and this will describe that weather particulate will settle down in aggregate form or as discrete grains. Flocculation can influence the deposition of clay and silt particles. The ratio of silt and clay can describe the interaction of sediment and water during hydrate formation. This ratio is also related to the particle size distribution [50]. The sediments from KG basin contains more clays minerals as compared to other sediment samples. The hydrate-bearing sediment samples from the Mahanadi and KK basins mainly contain silt particles. The available amount of clay and silt particles in hydrate-bearing sediment samples can affect the hydrate formation conditions and hydrate content due to their particle sizes. The sediment from the KG and KK basins contains fine particles that vary from clay to silt. The sediment from the KG basin contains a higher amount of sand than other sediment samples. The presence of sand can affect the hydrate formation in the sediments of the KG basin. The sediment from the Mahanadi basin contains a minimum amount of sand.

Table 4. Percentage of clay, silt, and sand particles in sediment samples.

Sediments	Sand (%)	Silt (%)	Clay-Size (%)	Sediments	Sand (%)	Silt (%)	Clay-Size (%)
KG(1a)	3.35	43.76	52.01	KK	0.43	54.09	45.42
KG(1b)	2.37	51.23	46.29	Mahanadi	0.12	61.07	38.73

3.3. X-ray Diffraction (XRD)

The powdered XRD analysis was conducted as given in [44]. Figure 4 shows the diffractogram for X-ray diffraction. The mineral component of the hydrate-bearing sediments was sepiolite (S), quartz (Q), magnetite (M), kaolinite (K), halite syn (H), and calcite (C). The agglomeration and nucleation behavior of sediments containing hydrate changes according to the type of minerals. The swelling and flow behavior of clay is affected by the water adsorption efficiency of minerals existed in the sediments. The identified list of minerals in the sediments has been analyzed by XRD interpretation software MATCH (CRYSTAL IMPACT). The list of minerals and their approximate percentage observed in the XRD Diffractogram is given in Table 5.

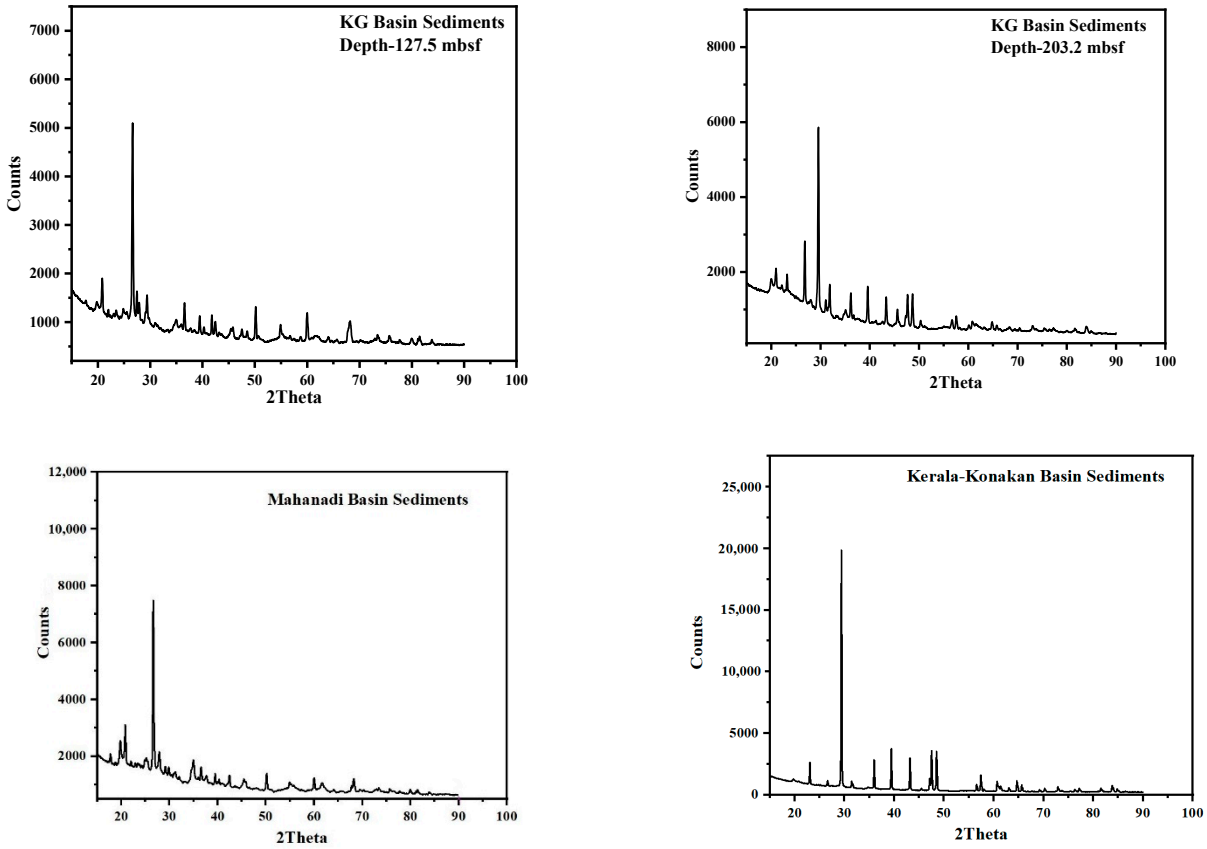

Figure 4. XRD Diffractogram.

Table 5. Approximate percentage of minerals observed in the XRD Diffractogram.

Minerals	PDF Index Name	Chemical Formula	2θ	Percentage			
				KG(1a)	KG(1a)	Mahanadi	KK
Quartz, syn	Silicon Oxide	SiO_2	26.652 26.640	66.34	66.88	62.81	69.37
Calcite, syn	Calcium Carbonate	$CaCO_3$	29.406	10.9	11.09	11.2	9.87
Halite, syn	Sodium Chloride	NaCl	31.693	7.91	8.20	8.3	6.76
Hematite	Iron Oxide	Fe_2O_3	33.115	5.1	5.7	6.8	4.7
Silicon, syn	Silicon	Si	28.443	2.3	1.87	2.31	2.11
Bornite	Copper Iron Sulfide	Cu_5FeS_4	46.945	1.9	1.63	1.89	1.01
Eskolaite, syn	Chromium Oxide	Cr_2O_3	33.597	2.7	1.3	1.65	1.78
Fluorite, syn	Calcium Fluoride	CaF_2	47.005	1.2	1.04	2.09	1.87
Chromium, syn	Chromium	Cr	44.393	0.7	1.01	2.1	0.91
Corundum, syn	Aluminum Oxide	Al_2O_3	43.363	0.5	0.3	0.6	0.67

The mineral composition of hydrate-bearing sediment samples and the chemical description of all minerals is given in Table 5. The percentage of quartz was maximum in all hydrate-bearing sediment samples. The main minerals observed in sediment samples were Calcite, Halite, Silicon, Hematite, and Bornite. Halite minerals are highly soluble in water. After performing the XRD analysis of the dried and wet hydrate-bearing sediment samples, we observed that approximately 64% the halite was present in dissolved form and 36% of the halite was in mineral form in all sediment samples.

The presence of clay in hydrate-bearing sediments reduces the void spaces and can then decrease the conversion of water to hydrate and the rate of hydrate formation. Therefore, Bentonite clay can inhibit the growth of hydrate in the sediments [51]. The accumulations of hydrate can be observed in coarse-grained sand in which the pore connectivity is good, which can lead to the even distribution of gas throughout. The high number of clay particles decreases the pore space and the accumulation of hydrates. The presence of Kaolin clay may inhibit the formation of methane hydrate [52].

3.4. Fourier Transform Infrared Spectroscopy

The infrared spectra of hydrate-bearing sediment samples have been shown in Figure 5. carbonate and quartz were detected in all the sediment samples. The peaks are detected at 1638–1641, 1439, 1033–1034, 792.9–797.3, 694.7, and 525.8–526.9 cm^{-1} in a sediment sample from the Mahanadi and Kerala-Konkan basin and confirm the existence of carbonate, silicate, and quartz. In the sediment sample from the Krishna-Godavari basin and Andaman basin [44], the observed peaks confirm the presence of smectite, kaolinite, silica, quartz carbonate, and silicate. Smectite is detected in the sediment sample from the Krishna-Godavari basin at a depth of 127.5 mbsf. Moreover, it is detected in the sediment sample from the Krishna-Godavari basin at a depth of 203.2 mbsf. The list of minerals and their wave number observed in the FTIR analysis is given in Table 6.

Table 6. Minerals and their wave number observed in the FTIR analysis.

Wave Number (cm^{-1})	792.9	1439	1150–1270	1034	875	2840–2960	490	525.8	1638	3458
Minerals Bond	Quartz	Carbonate C=O	Silica Si-O-Si	Kaolinite	Calcite	C-H	Si-O	Si-O-Al	Al-O-H	Smectite

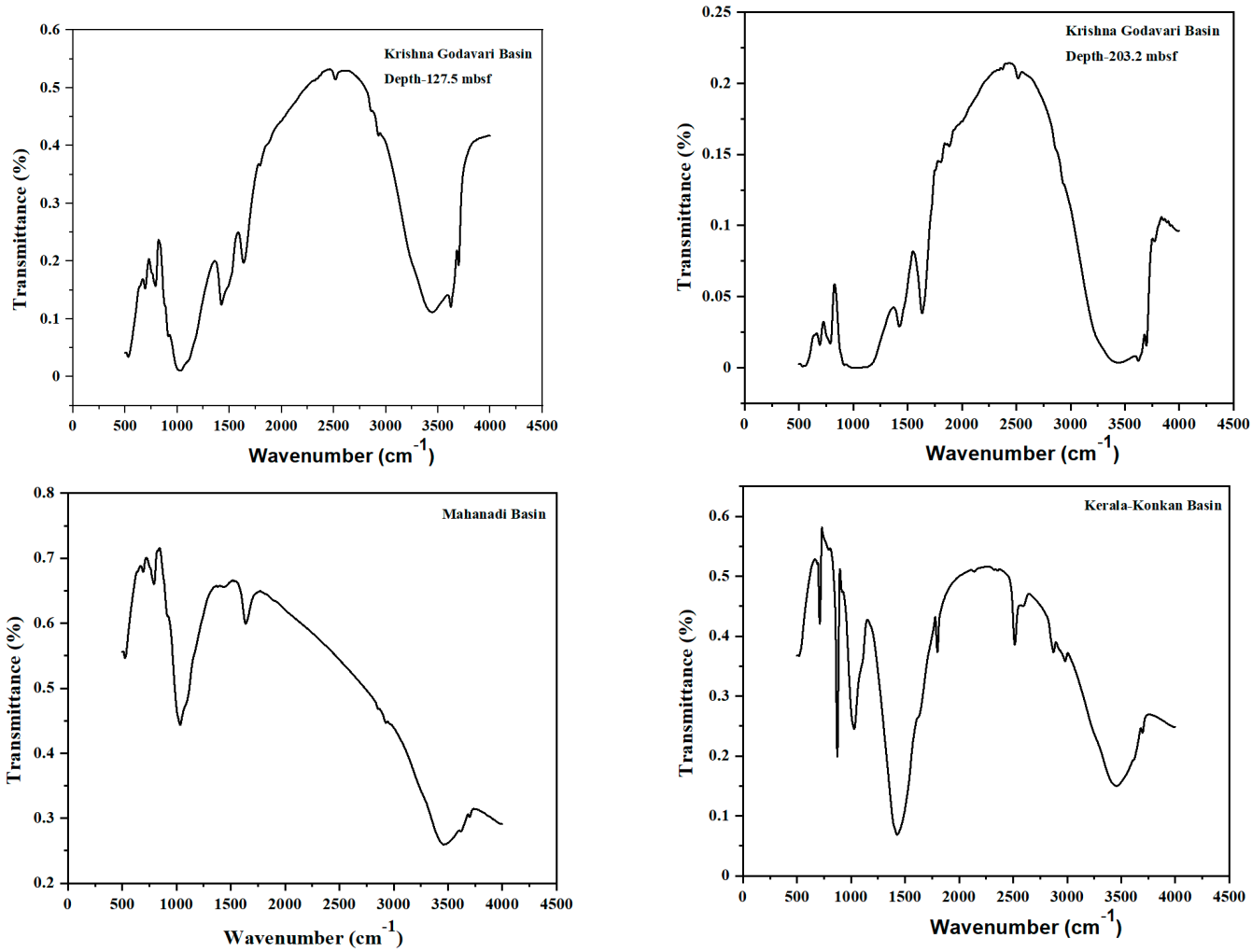

Figure 5. FTIR analysis.

3.5. Raman Spectra

The Raman spectra for gas hydrate-bearing sediment samples from the Krishna-Godavari, Mahanadi, and Kerala-Konkan basins are shown in Figure 6. The Raman spectra for all sediment samples was conducted as explained in [44]. The specific mineral peaks observed in the Raman spectra are compared with Renishaw's Inorganic Material and Minerals Database.

The gas hydrate-bearing sediments primarily contain quartz, kaolinite, silica, calcite, halite, silicon, bornite, and hematite. The strong peaks identified at 495 cm^{-1} and 1345 cm^{-1} in the Raman Spectra of the Krishna-Godavari basin confirm the presence of quartz; however, the weak peaks at 160, 310, and 1075 cm^{-1} confirm the presence of calcite. The strong peak observed at 1598 cm^{-1} shows the characteristics of the carbon D and G bonds of amorphous carbon. The strong peaks identified at 1450 cm^{-1} in the Raman Spectra of the Kerala-Konkan basin confirm the presence of hematite, but the weak peaks at 515 cm^{-1} confirm the presence of quartz. The sediment sample from the Mahanadi basin and the Andaman basin [44] shows the very small peaks for quartz and other minerals.

The growth and formation of gas hydrate formed in sediments will be affected by the presence of different types of minerals. The swelling behavior of the sediments depends on the water adsorption efficiency of the minerals present in the host sediments. Mineralogical constituents also influence the flow behavior of fine sediments. Table 7 shows the minerals available in the sediment samples and the corresponding characteristics peaks of the Raman spectra.

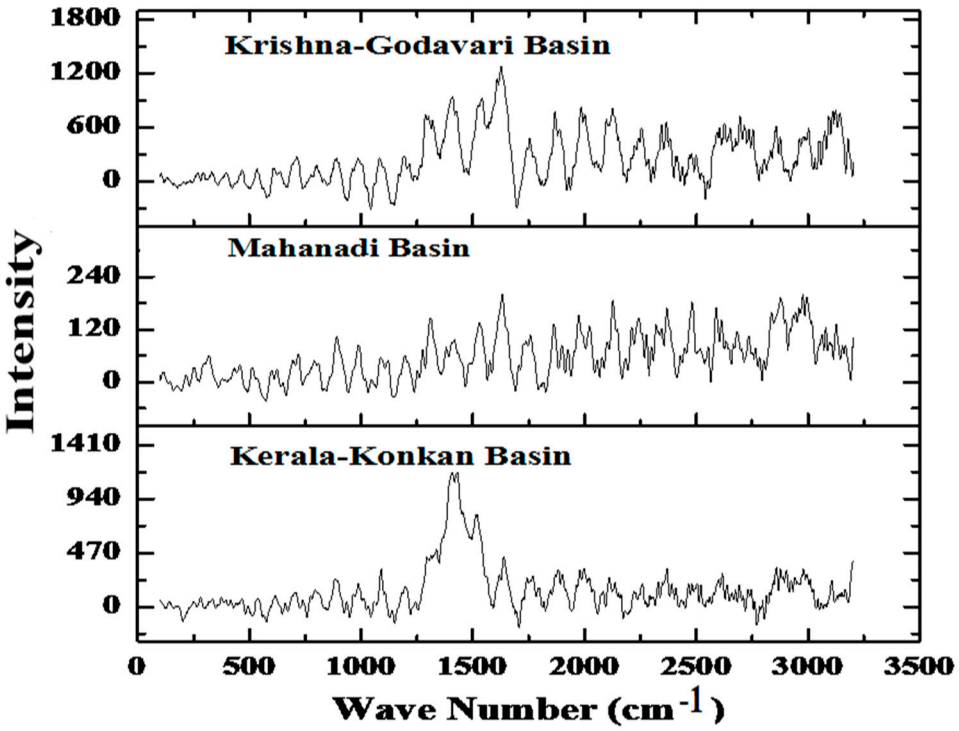

Figure 6. Raman spectra of hydrate-bearing sediment samples.

Table 7. Mineralogical and chemical properties of sediment samples [53] with permission from Elsevier, 2000.

Minerals	Chemical Formulation	Color	Characteraistics of Raman Bands (cm^{-1})
Quartz	SiO_2	Colourless	148, 357, 465, 1300–1600
Kaolinite	Al_2O_3 $2SiO_2 \cdot 2H_2O$	White	130, 143, 245, 270, 336, 394, 418, 431, 463, 3651, 3620, 3669
Hematite	Fe_2O_3	Red	224, 244, 290, 292, 409, 610, 670, 1300
Calcite	$CaCO_3$	White	154, 282, 712 1086, 1088
Halite	NaCl	Colourless	199
Silicon	Si	Blue-Grey Metallic	480, 520
Bornite	Cu_5FeS_4	Copper Red, Bronze Brown, Purple	265, 291, 320, 354, 470, 472

3.6. Inductively Coupled Plasma Mass Spectrometry (ICPMS)

The result obtained by the ICPMS analysis is given in Table 8. The manganese, potassium, and iron content in the sediment samples from the KG and Mahanadi basin are very high. The amount of copper and aluminum is high in the sediment samples from the Mahanadi basin. The silicon content in the sediment samples from the KG basin at different depths shows the minimum and maximum values. It confirms that the amount of silicon varies with the depth in the KG basin. The titanium concentration in all sediment samples is low, but samples from the KK basin contain titanium in high concentrations as compared to sediment samples from other basins. The iron concentration in sediment samples confirms the presence of bornite and hematite, and the aluminum concentration confirms the presence of corundum. The zinc content is high in hydrate-bearing sediments from the Andaman basin as compare to other samples [44]. The concentration of these chemicals can affect the formation and dissociation condition of gas hydrate in sediments. The particulate matter origination of the sediment sample, the reaction between the chemicals and the dissolved phase in the transport, and the displacement can be represented by the chemical proportions of hydrate-bearing sediment samples. The detrital and organic mineral supply can be indicated by the Al in the sediment sample. The hydrate-bearing sediment sample

from the KG(1a) basin has a higher Al concentration and shows a higher supply of organic and detrital matter, which shows the lower supply of detrital and organic matter in the sediment. The existence of K, Si, Mg, Fe, and Cu confirms the presence of feldspar, hematite, quartz, bornite, and illite, respectively.

Table 8. Chemical analysis of sediment samples.

Sediments Sample	Zn ppm	Mg ppm	Fe Ppm	Cu ppm	K ppm	Mn ppm	Al ppm	Si ppm	Ti ppm
KG(1a)	54.5468	429.3818	6459.293	12.3342	1152.639	126.0628	3025.748	0.2338	0.6332
KG(1b)	21.6668	361.3846	2291.756	5.2406	582.3844	43.349	1286.133	16.842	1.1428
Mahanadi	48.9012	403.0738	4259.515	122.473	777.1196	47.5806	2258.604	6.5728	0.859
KK	18.6542	274.9	1153.634	4.282	441.7348	99.0292	1008.338	8.9012	3.61

3.7. Specific Surface Areas and Cation Exchange Capacities

The value of the specific surface area and CEC is shown in Table 9. The Cation Exchange Capacity depends on the clay minerals, while the specific surface area is mainly governed by the size of particles as well as their clay minerals. The higher CEC value indicates the presence of a more significant fraction of clay minerals. The order of specific surface area and CEC for hydrate-bearing sediments from different natural deposits of India are Mahanadi > KG(1b) > Andaman [44] > KG(1a) > KK. The CEC values between 3–15 meq/100 g confirm the presence of kaolinite and quartz in the hydrate-bearing sediments. The specific surface area of the clay mineral is high as compared to their weight. Hence, they are easy to bind with one another and also to other materials present in the water [54]. This was also stated in [54], where the precipitated silt and clay minerals were distinguished by their high specific surface The specific surface area of the hydrate-bearing sediments from the Mahanadi basin is higher than the KG basin because the sediments from the Mahanadi basin contain a higher percentage of silt and clay minerals. The specific surface area denotes the dissipation degree of the sediments and also inversely depends on the size of the particle. The specific surface area of the hydrate-bearing sediments is 20 m^2/g. Table 9 also shows the particle size of clay minerals and their percentage observed in the sediment samples. The sediment samples contain a higher amount of illite than kaolinite and smectite. Illite can affect the formation of hydrates in sediments because it can hold more water.

Table 9. Specific Surface Areas (SA) and Cation Exchange Capacities (CEC) of sediments.

Sediments Sample	Particle Size (μm)			Clay Mineral and Content (%)			Specific Surface Area (m^2/g)	Cation Exchange Capacities (meq/100 g)
	Kaolinite	Smectite	Illite	Kaolinite	Smectite	Illite		
KG(1a)	0.38–0.86	0.9–2.4	0.03–0.08	14.7	6.4	68.9	20.1	8.062
KG(1b)				15.1	6.7	65.6	22.1	5.498
Mahanadi				16.3	7.4	66.3	43.2	8.588
KK				12.8	5.9	59.2	19.0	7.228

3.8. Scanning Electron Microscopy (SEM)

The physical properties of the sediment sample were performed as given in Kumari et al. 2021 [43]. Figure 7 indicates the SEM images and Energy Dispersive Spectroscopy (EDS) graph of sediment samples from the different basins. The sediment sample from KG and Konkan basin has an aggregate-like structure, which shows the presence of strong van der Waals forces. These van der Waals forces hold each clay particle together and form floccules. The sediment sample from the Mahanadi basin and Andaman basin [44] does not show the dispersed-like structure, which shows that there will be weak van der Waal

forces. The surface texture and sediment geometry can influence the mechanical properties of the hydrate-bearing sediments [14].

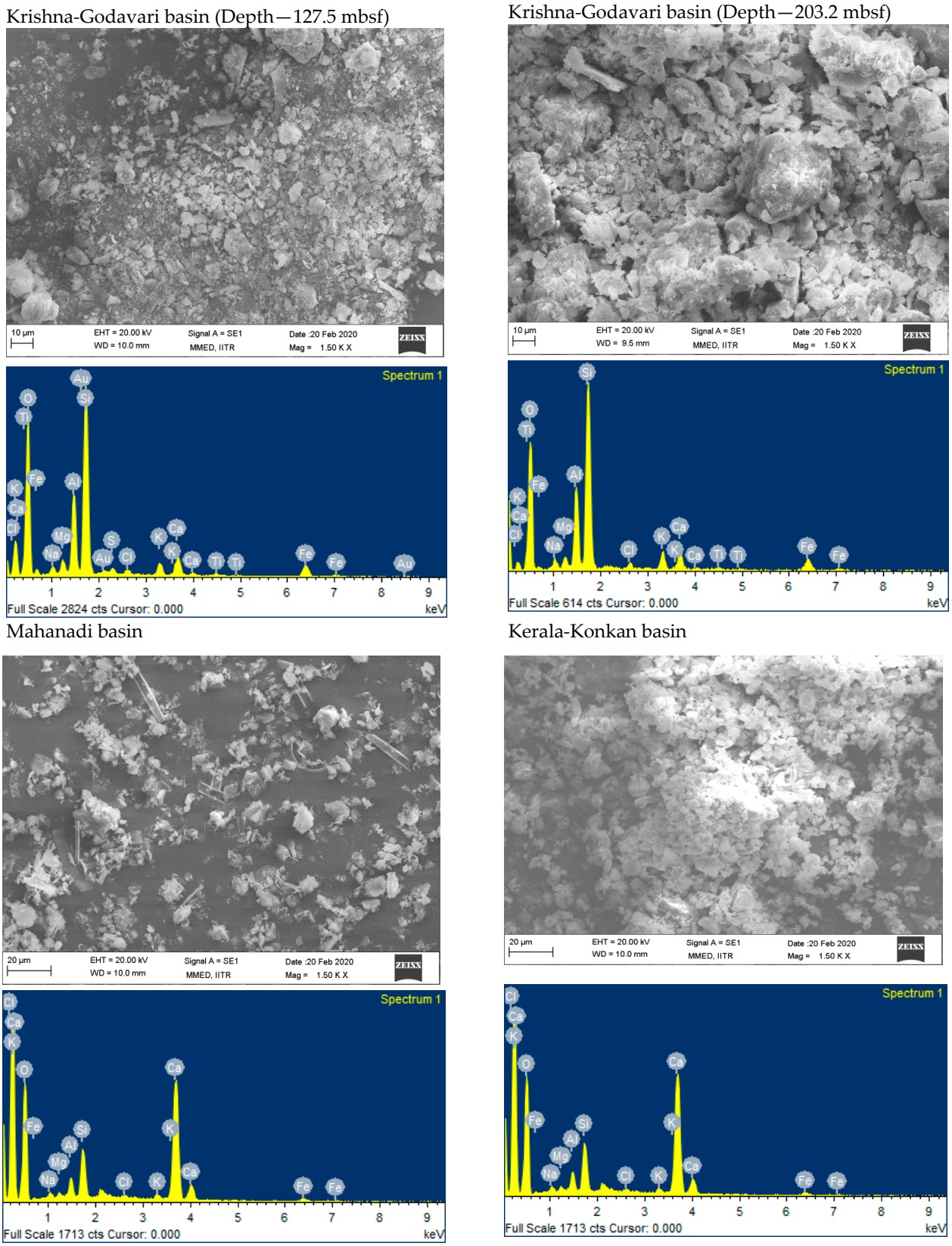

Figure 7. Analysis of SEM and EDS for hydrate-bearing sediment samples.

The EDS graph confirmed the existence of O, Na, Mg, Si, Al, S, Cl, K, Ca, Au, and Fe. The sediment sample from the KG basin at a depth of 127.5 mbsf contains all of the above elements, but the KG basin at a depth of 203.2 mbsf does not contain S and Au. Moreover, the Mahanadi basin does not contain S, Ca, and Au, the Kerala-Kankan basin does not contain S and Au, and the Andaman basin does not contain Mg, S, and Au [44]. The existence of elements Al, Mg, K, Si, and Fe increases the cementation properties of the clay particles, as shown in Figure 7 The elemental analysis of the sample is given in Table 10. Due to the presence of diatoms in marine sediments, the internal pore of the sediments will be increased, and hence, it will decrease the specific gravity and increase the specific surface area and porosity. The sediments particles are mostly in the face-to-face flake form and display a dispersed structure, which indicates the anisotropic character of the marine sediments.

Table 10. Elemental analysis of hydrate-bearing sediment samples.

Elements (wt. %)	Krishna-Godavari Basin Depth—127.5 mbsf	Krishna-Godavari Basin Depth—203.2 mbsf	Mahanadi Basin	Kerala-Konkan Basin
O	60.05	53.54	67.11	67.09
Na	1.22	1.47	1.61	0.82
Mg	1.32	1.09	1.23	0.62
Al	6.89	8.82	6.23	2.03
Si	16.31	23.36	18.41	5.74
S	1.02	—-	—-	—-
Cl	0.69	0.90	0.66	0.42
K	1.73	3.11	2.04	0.61
Ca	4.60	2.55	—-	21.44
Au	2.56	—-	—-	—-
Fe	3.61	5.17	2.70	1.23

The chemical and physical properties of hydrate-bearing sediments will play an important role in improving hydrate dissociation methods. The depressurization methods have the limitation of mechanical properties of sediments, and this study can help improve the mechanical stability of the gas hydrate reservoir. Thermal stimulation has the drawback of poor recovery efficiency, and hence, it can influence the hydraulic stability of the reservoirs. Thus, knowledge of the physical and chemical properties of the sediments can control hydraulic failures. Similarly, the efficiency of the CO_2 sequestration method can also be improved by the prediction of these properties.

From a scientific perspective, the sediments from the KG basin sites need to be the focus of future studies, as these can clarify the formations of gas hydrates at real gas hydrates sites and assist in the arrangement of new methods for the gas hydrate dissociation. Moreover, the current study has considered various physical and chemical properties of sediments at various Indian locations and the properties studied above can serve as a guiding tool for designing a dissociation technology for gas hydrates from hydrate-bearing sediments, as the properties studied above will guide the thermal phenomenon influencing the production parameters, such as heat transfer from adjacent formations. Salinity is directly related to the efficiency of gas production. The migration of particles to wells can destruct the gas flow. The EDS analysis has given an idea about the various elements present in the sediments. The detailed mineralogy of various samples of sediments was depicted by various techniques, such as XRD, FTIR, and Raman Spectroscopy, giving a detailed idea of the mineralogy of various gas hydrates formed in Indian reservoirs The fine-grained sediment's flow behavior significantly depends on the mineralogy of the clay samples [55]. Specific surface area is a type of mineralogical index depicting the mechanical as well as electrical properties of sediments, which will be the guiding parameters for designing any dissociation technique. The SEM has depicted the morphology of sediments, which in turn influence the mechanical properties of the sediments.

The above study has cleared the role of various sediments for the formation of gas hydrates at various Indian Gas hydrates sites, as well as knowledge of their various physical and chemical properties and their significance in designing future gas hydrate dissociation technologies which are needed for the commercialization of this vast resource of energy.

4. Conclusions

In this study, sediment samples were taken from the Mahanadi basin (Depth—217.4 mbsf, Hydrate Saturation—>50%, Sea Floor Temperature—2.4 °C), Kerala-Konkan basin (Depth—246.8 mbsf, Hydrate Saturation—15%), and Krishna-Godavari basin (Depth—127.5 and 203.2 mbsf, Hydrate Saturation—3 to 39%), recovered during the National Gas Hydrate Program I and II. The physical characteristics of hydrate-bearing sediments from Indian-origin reservoirs provided important information for the intrinsic behavior of host sediment. The data from particle size confirmed the distribution of clay and silt. Quartz is the main mineral (66.8% approx.) observed in the gas hydrate-bearing sediments. Iron is the main component observed in the sediment samples (2000 to 6000 ppm). The specific surface area was higher for the sediment sample from the Mahanadi basin, representing the sediments' dissipation degree. The sediments from the Krishna-Godavari basin are mainly clay, in addition to limited sand/silt bed type, but the sediments from the Mahanadi basin are not of silt/sand bed type. The gas hydrate-bearing sediments from the Kerala-Konkan basin are of carbonate-rich type. The particle size of the sediment samples affects the induction and growth rate of hydrates. The presence of clay in hydrate-bearing sediments reduces the void spaces and can then decreases the conversion of water to hydrate and the rate of hydrate formation. The growth and formation of gas hydrate formed in sediments will be affected by the presence of different types of minerals. The aggregate-like structure of the sediment samples indicates the van der Waals forces; hence, the clay particles can hold each other and can influence the hydrate content. The physio-chemical characteristics evaluated for hydrate-bearing sediments of various Indian basins can help in removing various limitations possessed by each dissociation method currently, such as depressurization, thermal stimulation, inhibitor injection, and CO_2 sequestration. These characteristics can be used to design a new economical gas hydrate dissociation technology which can give better results compared to the available hydrate dissociation technologies. The current study gives detailed ideas about the physical, chemical, and mineralogical characteristics of gas hydrate-bearing sediments which can affect the efficiency of hydrate formation and dissociation in sediments. Hence, this study can become a helpful tool for taking energy from fiery ice and can turn it into a future generation fuel.

Author Contributions: Conceptualization, methodology, formal analysis, investigation, resources, data curation, writing—original draft preparation, A.K.; writing—review and editing, S.R.G. and A.A.; visualization, supervision, C.B.; project administration, funding acquisition, G.D. All authors have read and agreed to the published version of the manuscript.

Funding: This research was funded by Gas Hydrate Research & Technology Centre (GHRTC) through the Oil and Natural Gas (ONGC), PANVEL and Ministry of Human Resource Development (MHRD), India, grant number-ONG-1160-CHD-17/18.

Institutional Review Board Statement: Not applicable.

Informed Consent Statement: Not applicable.

Acknowledgments: This work is supported by the Gas Hydrate Research & Technology Centre (GHRTC) through the Oil and Natural Gas (ONGC), PANVEL and Ministry of Human Resource Development (MHRD), India.

Conflicts of Interest: The authors declare no conflict of interest.

References

1. Lee, J.Y.; Kim, G.Y.; Kang, N.K.; Yi, B.Y.; Jung, J.W.; Im, J.H.; Son, B.K.; Bahk, J.J.; Chun, J.H.; Ryu, B.J.; et al. Physical properties of sediments from the Ulleung Basin, East Sea: Results from Second Ulleung Basin Gas Hydrate Drilling Expedition, East Sea (Korea). *Mar. Pet. Geol.* **2013**, *47*, 43–55. [CrossRef]
2. Arora, A.; Cameotra, S.S.; Kumar, R.; Balomajumder, C.; Singh, A.K.; Santhakumari, B.; Kumar, P.; Laik, S. Biosurfactant as a Promoter of Methane Hydrate Formation: Thermodynamic and Kinetic Studies. *Sci. Rep.* **2016**, *6*, 1–13. [CrossRef] [PubMed]
3. Khan, S.H.; Kumari, A.; Chandrajit, G.D.; Amit, B.M. Thermodynamic modeling and correlations of CH_4, C_2H_6, CO_2, H_2S, and N_2 hydrates with cage occupancies. *J. Pet. Explor. Prod. Technol.* **2020**. [CrossRef]
4. Kvenvolden, K.A. A primer on the geological occurrence of gas hydrate. *Geol. Soc. Lond. Spec. Publ.* **1998**, *137*, 9–30. [CrossRef]
5. Bei, K.; Xu, T.; Shang, S.; Wei, Z.; Yuan, Y.; Tian, H. Numerical Modeling of Gas Migration and Hydrate Formation in Heterogeneous Marine Sediments. *J. Mar. Sci. Eng.* **2019**, *7*, 348. [CrossRef]
6. Ecker, C.; Dvorkin, J.; Nur, A. Sediments with gas hydrates: Internal structure from seismic AVO. *Geophysics* **1998**, *63*, 1659–1669. [CrossRef]
7. Arora Swaranjit Singh, A.; Chandrajit, C. Natural Gas Hydrate (Clathrates) as an Untapped Resource of Natural Gas. 2015, Volume 6. Available online: https://www.longdom.org/open-access/natural-gas-hydrate-clathrates-as-an-untapped-resource-of-natural-gas-2157-7463-1000234.pdf (accessed on 26 July 2021).
8. Kumari, A.; Khan, S.H.; Misra, A.K.; Majumder, C.B.; Arora, A. Hydrates of Binary Guest Mixtures: Fugacity Model Development and Experimental Validation. *J. Non-Equilib. Thermodyn.* **2020**, *45*, 39–58. [CrossRef]
9. Miyawaki, J.; Kanda, T.; Suzuki, T.; Okui, T.; Maeda, Y.; Kaneko, K. Macroscopic evidence of enhanced formation of methane nanohydrates in hydrophobic nanospaces. *J. Phys. Chem. B* **1998**, *102*, 2187–2192. [CrossRef]
10. Arora, A.; Cameotra, S.S. Techniques for exploitation of gas hydrate (clathrates) an untapped resource of methane gas. *J. Microb. Biochem. Technol.* **2015**, *7*. [CrossRef]
11. Arora, A.; Kumar, A.; Bhattacharjee, G.; Kumar, P.; Balomajumder, C. Effect of different fixed bed media on the performance of sodium dodecyl sulfate for hydrate based CO_2 capture. *Mater. Des.* **2016**, *90*, 1186–1191. [CrossRef]
12. MORK, M.; SCHEI, G.; LARSEN, R. NMR Imaging Study of Hydrates in Sediments. *Ann. N. Y. Acad. Sci.* **2006**, *912*, 897–905. [CrossRef]
13. Bahk, J.J.; Kim, D.H.; Chun, J.H.; Son, B.K.; Kim, J.H.; Ryu, B.J.; Torres, M.E.; Riedel, M.; Schultheiss, P. Gas hydrate occurrences and their relation to host sediment properties: Results from Second Ulleung Basin Gas Hydrate Drilling Expedition, East Sea. *Mar. Pet. Geol.* **2013**, *47*, 21–29. [CrossRef]
14. Kwon, T.H.; Lee, K.R.; Cho, G.C.; Lee, J.Y. Geotechnical properties of deep oceanic sediments recovered from the hydrate occurrence regions in the Ulleung Basin, East Sea, offshore Korea. *Mar. Pet. Geol.* **2011**, *28*, 1870–1883. [CrossRef]
15. Winters, W.J.; Wilcox-Cline, R.W.; Long, P.; Dewri, S.K.; Kumar, P.; Stern, L.; Kerr, L. Comparison of the physical and geotechnical properties of gas-hydrate-bearing sediments from offshore India and other gas-hydrate-reservoir systems. *Mar. Pet. Geol.* **2014**, *58*, 139–167. [CrossRef]
16. Nair, V.C.; Prasad, S.K.; Sangwai, J.S. Characterization and Rheology of Krishna-Godavari basin Sediments. *Mar. Pet. Geol.* **2019**, *110*, 275–286. [CrossRef]
17. Jang, J.; Waite, W.F.; Stern, L.A.; Collett, T.S.; Kumar, P. Physical property characteristics of gas hydrate-bearing reservoir and associated seal sediments collected during NGHP-02 in the Krishna-Godavari Basin, in the offshore of India. *Mar. Pet. Geol.* **2019**, *108*, 249–271. [CrossRef]
18. Dong, L.; Li, Y.; Liao, H.; Liu, C.; Chen, Q.; Hu, G.; Liu, L.; Meng, Q. Strength estimation for hydrate-bearing sediments based on triaxial shearing tests. *J. Pet. Sci. Eng.* **2020**, *184*, 106478. [CrossRef]
19. Gabitto, J.F.; Tsouris, C. Physical Properties of Gas Hydrates: A Review. *J. Thermodyn.* **2010**, *2010*, 271291. [CrossRef]
20. Stoll, R.D.; Bryan, G.M. Physical Properties of Sediments Containing Gas Hydrates. *J. Geophys. Res.* **1979**, *84*, 1629–1634. [CrossRef]
21. Mahabadi, N.; Dai, S.; Seol, Y.; Jang, J. Impact of hydrate saturation on water permeability in hydrate-bearing sediments. *J. Pet. Sci. Eng.* **2019**, *174*, 696–703. [CrossRef]
22. Wang, L.; Li, Y.; Wu, P.; Shen, S.; Liu, T.; Leng, S.; Chang, Y.; Zhao, J. Physical and mechanical properties of the overburden layer on gas hydrate-bearing sediments of the South China sea. *J. Pet. Sci. Eng.* **2020**, *189*, 107020. [CrossRef]
23. Lee, K.M.; Lee, H.; Lee, J.; Kang, J.M. CO_2 hydrate behavior in the deep ocean sediments; phase equilibrium, formation kinetics, and solubility. *Geophys. Res. Lett.* **2002**, *29*, 30–31. [CrossRef]
24. Cha, S.B.; Ouar, H.; Wildeman, T.R.; Sloan, E.D. A third-surface effect on hydrate formation. *J. Phys. Chem.* **1988**, *92*, 6492–6494. [CrossRef]
25. Yuan, Q.; Kong, L.; Xu, R.; Zhao, Y. A State-Dependent Constitutive Model for Gas Hydrate-Bearing Sediments Considering Cementing Effect. *J. Mar. Sci. Eng.* **2020**, *8*, 621. [CrossRef]
26. Uchida, T.; Takeya, S.; Chuvilin, E.M.; Ohmura, R.; Nagao, J.; Yakushev, V.S.; Istomin, V.A.; Minagawa, H.; Ebinuma, T.; Narita, H. Decomposition of methane hydrates in sand, sandstone, clays and glass beads. *J. Geophys. Res. Solid Earth* **2004**, *109*, 1–12. [CrossRef]
27. Winters, W.J.; Pecher, I.A.; Waite, W.F.; Mason, D.H. Physical properties and rock physics models of sediment containing natural and laboratory-formed methane gas hydrate. *Am. Mineral.* **2004**, *89*, 1221–1227. [CrossRef]

28. Sun, X.; Wang, L.; Luo, H.; Song, Y.; Li, Y. Numerical modeling for the mechanical behavior of marine gas hydrate-bearing sediments during hydrate production by depressurization. *J. Pet. Sci. Eng.* **2019**, *177*, 971–982. [CrossRef]
29. Hyodo, M.; Li, Y.; Yoneda, J.; Nakata, Y.; Yoshimoto, N.; Kajiyama, S.; Nishimura, A.; Song, Y. A comparative analysis of the mechanical behavior of carbon dioxide and methane hydrate-bearing sediments. *Am. Mineral.* **2014**, *99*, 178–183. [CrossRef]
30. Zhang, Q.; Li, F.G.; Sun, C.Y.; Li, Q.P.; Wu, X.Y.; Liu, B.; Chen, G.J. Compressional wave velocity measurements through sandy sediments containing methane hydrate. *Am. Mineral.* **2011**, *96*, 1425–1432. [CrossRef]
31. Collett, T.S.; Boswell, R.; Cochran, J.R.; Kumar, P.; Lall, M.; Mazumdar, A.; Ramana, M.V.; Ramprasad, T.; Riedel, M.; Sain, K.; et al. Geologic implications of gas hydrates in the offshore of India: Results of the National Gas Hydrate Program Expedition 01. *Mar. Pet. Geol.* **2014**, *58*, 3–28. [CrossRef]
32. Gao, Y.; Yang, M.; Zheng, J.N.; Chen, B. Production characteristics of two class water-excess methane hydrate deposits during depressurization. *Fuel* **2018**, *232*, 99–107. [CrossRef]
33. Hyndman, R.D.; Spence, G.D. A seismic study of methane hydrate marine bottom simulating reflectors. *J. Geophys. Res.* **1992**, *97*, 6683–6698. [CrossRef]
34. Sloan, E.D.; Koh, C.A. *Clathrate Hydrates of Natural Gases*, 3rd ed.; Chemical Industries Series pdf; CRC Press: Boca Raton, FL, USA, 1998; Available online: https://www.routledge.com/Clathrate-Hydrates-of-Natural-Gases/Sloan-Jr-Koh-Koh/p/book/9780849390784 (accessed on 26 July 2021).
35. Tinivella, U.; Giustiniani, M. Variations in BSR depth due to gas hydrate stability versus pore pressure. *Glob. Planet. Chang.* **2013**, *100*, 119–128. [CrossRef]
36. Shankar, U.; Sain, K.; Riedel, M. Geothermal modeling for the base of gas hydrate stability zone and saturation of gas hydrate in the Krishna-Godavari basin, eastern Indian margin. *J. Geol. Soc. India* **2012**, *79*, 199–209. [CrossRef]
37. Nur, A. BSR and Methane Hydrates: New Challenges for Geophysics and Rock Physics. In Proceedings of the Offshore Technology Conference, Houston, TX, USA, 6–9 May 1996; pp. 429–435.
38. Krishna Godavari–Basin | NDR (National Data Repository)-Directorate General of Hydrocarbons(DGH) | Ministry of Petroleum and Natural Gas, Government of India. 2015. Available online: https://www.ndrdgh.gov.in/NDR/?page_id=647 (accessed on 27 July 2021).
39. Kumar, P.; Collett, T.S.; Boswell, R.; Cochran, J.R.; Lall, M.; Mazumdar, A.; Ramana, M.V.; Ramprasad, T.; Riedel, M.; Sain, K.; et al. Geologic implications of gas hydrates in the offshore of India: Krishna-Godavari Basin, Mahanadi Basin, Andaman Sea, Kerala-Konkan Basin. *Mar. Pet. Geol.* **2014**, *58*, 29–98. [CrossRef]
40. Campanile, D.; Nambiar, C.G.; Bishop, P.; Widdowson, M.; Brown, R. Sedimentation record in the Konkan-Kerala Basin: Implications for the evolution of the Western Ghats and the Western Indian passive margin. *Basin Res.* **2008**, *20*, 3–22. [CrossRef]
41. Mishra, S.; Verma, R.; Silva, K.D.; Banerjee, S.; Bastia, R.; Nathaniel, D.M. Sub-Basalt Hydrocarbon Prospectivity in Kerala-Konkan Offshore Basin, India: A Basin Modeling Approach. *Search Discov.* **2011**, *30157*, 1–7.
42. Kamesh Raju, K.A.; Ramprasad, T.; Rao, P.S.; Ramalingeswara Rao, B.; Varghese, J. New insights into the tectonic evolution of the Andaman basin, northeast Indian Ocean. *Earth Planet. Sci. Lett.* **2004**, *221*, 145–162. [CrossRef]
43. Winters, W.J.; Novosel, I.; Boldina, O.; Waite, W.F.; Kelsey, S.A.; Hallett, B.W. Physical properties of sediment obtained during the IMAGES VIII/PAGE 127 gas hydrate and paleoclimate cruise on the RV Marion Dufresne in the Gulf of Mexico, 2–18 July 2002. In *Initial Report of the IMAGES VIII/PAGE 127 Gas Hydrate and Paleoclimate Cruise on the RV Marion Dufresne in the Gulf of Mexico, 2–18 July 2002*; US Geological Survey: Boulder, CO, USA, 2002; pp. 1–65. Available online: https://cmgds.marine.usgs.gov/publications/of2004-1358/pdf_chapters/Chapter4.pdf (accessed on 27 July 2021).
44. Kumari, A.; Hasan, S.; Majumder, K.C.B.; Arora, A.; Dixit, G. Physio-chemical and mineralogical analysis of gas hydrate bearing sediments of Andaman Basin. *Mar. Geophys. Res.* **2021**, 1–12. [CrossRef]
45. Sheard, R.W. Sand, Silt and Clay. Sport. Turf Newsl. Available online: https://www.sportsturfcanada.com/ (accessed on 26 July 2021).
46. Chibowski, E. *Flocculation and Dispersion Phenomena in Soils BT—Encyclopedia of Agrophysics*; Gliński, J., Horabik, J., Lipiec, J., Eds.; Springer: Dordrecht, The Netherlands, 2011; pp. 301–304. ISBN 978-90-481-3585-1.
47. Gallo, P.; Ricci, M.A.; Rovere, M. Layer analysis of the structure of water confined in vycor glass. *J. Chem. Phys.* **2002**, *116*, 342–346. [CrossRef]
48. Bouyoucos, G.J. Hydrometer Method Improved for Making Particle Size Analyses of Soils 1. *Agron. J.* **1962**, *54*, 464–465. [CrossRef]
49. Zhang, B.; Zhou, L.; Liu, C.; Zhang, Q.; Wu, Q.; Wu, Q.; Liu, C. Influence of sediment media with different particle sizes on the nucleation of gas hydrate. *Nat. Gas Ind. B* **2018**, *5*, 652–659. [CrossRef]
50. Sly, P.G. Sediment dispersion: Part 1, fine sediments and significance of the silt/clay ratio. *Hydrobiologia* **1989**, *176–177*, 99–110. [CrossRef]
51. Kumar, A.; Sakpal, T.; Roy, S.; Kumar, R. Methane hydrate formation in a test sediment of sand and clay at various levels of water saturation. *Can. J. Chem.* **2015**, *93*, 874–881. [CrossRef]
52. Bello-Palacios, A.; Almenningen, S.; Fotland, P.; Ersland, G. Experimental and Numerical Analysis of the Effects of Clay Content on CH4 Hydrate Formation in Sand. *Energy Fuels* **2021**, *35*, 9836–9846. [CrossRef]
53. Edwards, H.G.M.; Newton, E.M.; Russ, J. Russ Raman Spectroscopic Analysis of Pigments and Substrata in Prehistoric Rock Art. *J. Mol. Struct.* **2000**, *550–551*, 245–256. [CrossRef]

54. Dronkers, J.; van den Berg, J. Coastal and Marine Sediments. 2021. Available online: http://coastalwiki.org/wiki/Coastal_and_marine_sediments (accessed on 26 July 2021).
55. Jeong, S.W.; Locat, J.; Torrance, J.K.; Leroueil, S. Thixotropic and anti-thixotropic behaviors of fine-grained soils in various flocculated systems. *Eng. Geol.* **2015**, *196*, 119–125. [CrossRef]